PHYSICAL REVIEW B **74**, 174118 (2006)

Intermetallics in the Mg-Ca-Sn ternary system: Structural, vibrational, and thermodynamic properties from first principles

Raymundo Arróyave*
Department of Mechanical Engineering, Texas A&M University, College Station, Texas 77843, USA

Zi-Kui Liu
Department of Materials Science and Engineering, The Pennsylvania State University, University Park, Pennsylvania 16802, USA

(Received 1 May 2006; revised manuscript received 10 August 2006; published 22 November 2006)

A comprehensive analysis of the structural, vibrational, and thermodynamic properties of the intermetallic compounds in the Mg-Ca-Sn system has been performed via first-principles calculations. The enthalpies of formation at 0 K for all the known structures in this ternary system are calculated and the results are favorably compared—within ~5 kJ/mol-atom in most cases—to the available experimental data. The vibrational contributions to the thermodynamic properties of fcc Ca, hcp Mg, $\beta-$Sn, Mg_2Ca, Ca_2Sn, CaSn, Ca_5Sn_3, $CaSn_3$, Mg_2Sn, and MgCaSn are calculated using the supercell method. In all cases, bond stiffening resulting from compound formation results in upward frequency shifts in the phonon density of states, yielding in turn negative entropies of formation. The effects of volume expansion on the vibrational properties were considered through the quasiharmonic approximation. Thermal electronic contributions were also calculated from the electronic density of states. The electronic degrees of freedom were found to be less important than volume expansion at determining the high temperature thermodynamic properties. The predicted thermodynamic properties of the structures agreed satisfactorily with the experimental data available. The relative importance of these two nonharmonic corrections is reversed when analyzing the formation properties. In all compounds, except for $CaSn_3$, it was found that the variation of both the formation enthalpies and entropies with temperature is negative. This results in a destabilization of the compounds with respect to their constituent elements as the temperature is increased.

DOI: 10.1103/PhysRevB.74.174118 PACS number(s): 64.30.+t, 65.40.−b, 71.15.Nc, 71.20.Lp

I. INTRODUCTION

Some of the most common magnesium alloys are based on the Mg-Al binary. However, despite their high specific strength, these alloys have limited use as structural materials in automotive applications—especially in the engine bay—due to their poor creep resistance at temperatures above 120 °C (Ref. 1), mainly due to the softening of the intermetallic phase $Mg_{17}Al_{12}$ (Ref. 2) as temperature increases. Significant improvements can be achieved, however, by alloying. For example, calcium improves the creep resistance of Mg-Al alloys through the replacement of the detrimental $Mg_{17}Al_{12}$ compound by more stable Laves phases.[3–5] The replacement of this detrimental compound by the more stable Mg_2Sn can also be achieved through the addition of tin.[1]

Although there is certainly a potential for developing magnesium alloys better suited for high temperature operation, alloy development is a costly and time-consuming endeavor. Thankfully, computational approaches, such as the CALPHAD method,[6] have facilitated this process by allowing the prediction of phase stability and thermodynamic properties of alloys in regions of the composition-temperature space not yet accessed/accessible through experimental work.[7] The CALPHAD approach, however, is based on the evaluation of model parameters largely through experimental data and is therefore limited by the availability and quality of the latter. Recently, first-principles calculations have been used to provide some of the missing data necessary for thermodynamic modeling.[8–11]

In order to gain a better understanding of the alloying behavior of Ca and Sn on Mg-based alloys, it is important to determine the thermochemistry of the intermetallic compounds that exist in the Mg-Ca-Sn ternary. In the present paper, we present a detailed analysis of the structural, vibrational, and thermodynamic properties of the known intermetallic compounds in Mg-Ca-Sn via first-principles methods.

The enthalpies of formation of all the known phases in this system are calculated and compared with the available experiments. The ground state of the Ca-Sn binary—the Mg-Ca and Mg-Sn binaries have only one stable intermetallic compound—is then predicted and compared to the recent low-temperature phase diagram obtained by Palenzona *et al.*[12]

By using the force-constant—or supercell—method,[13] the vibrational properties of fcc Ca, hcp Mg, $\beta-$Sn, Mg_2Ca, Ca_2Sn, CaSn, Ca_5Sn_3, $CaSn_3$, Mg_2Sn, and MgCaSn are also calculated. The calculated phonon density of states (DOS) is subsequently used to calculate the vibrational contributions to the total free energy of the structures. To account for the effects of thermal expansion on the phonon DOS, the quasiharmonic correction is implemented. For structures of metallic character thermal electronic contributions (TEC) were taken into account.

It is important to note that in many cases, configurational degrees of freedom can play a significant role in determining the finite temperature thermodynamic properties of phases, with contributions that in some cases are greater than those due to vibrational effects. In this case, however, the solid phases exhibit almost negligible solubility ranges[14–16] and therefore the corresponding configurational effects can be neglected. Additional effects due to the formation, at high temperatures, of composition-conserving thermal point defects can safely be neglected in all but the highest melting compounds and thus they were not considered in this work.

Through the calculations outlined above, the thermochemical properties of these compounds—such as enthalpy, entropy, and specific heat—have been predicted and compared with the available experiments. Furthermore, structural properties, such as the bulk modulus are calculated as a function of temperature. The temperature dependence of the formation properties of the intermetallic compounds is calculated and the trends observed are interpreted in terms of the differences in the temperature dependence of the bulk moduli of the compounds, as well as a decrease of electronic disorder, relative to the reference structures. The results of this work are currently being used to develop a self-consistent CALPHAD thermodynamic model of the Mg-Ca-Sn ternary system.[14,17]

II. METHODOLOGY

A. Properties at $T=0$ K

The electronic structure and total energies of all the known compounds in the Mg-Ca-Sn system have been calculated using density functional theory, (DFT),[18] within both the local-density (LDA) and generalized-gradient approximations (GGA), using projector augmented-wave (PAW) pseudopotentials, as implemented in the Vienna *Ab initio* Simulation Package (VASP).[19–21] The LDA is implemented according to the Perdew-Zunger parametrization[22] of the data by Ceperly and Alder.[23] In the case of GGA, the generalized gradient corrections, PW91, have been used.[24] The atomic configurations considered were $3s^2\,3p^6\,4s^2$, $2p^6\,3s^2$, and $4d^{10}\,5s^2\,5p^2$ for Ca, Mg, and Sn, respectively.

During the structure optimization, all degrees of freedom were allowed to relax, and the Brillouin zone integrations were carried out using the Methfessel-Paxton order one smearing method.[25] After the relaxations, a final self-consistent static calculation with the tetrahedron smearing method with Blöchl corrections[26] was performed. An energy cutoff of 350 eV and a mesh of 1×10^4 k points per reciprocal atom, distributed isotropically, were used, resulting in a convergence of the total energies within a few meV.

B. Finite-temperature thermodynamics

In the case of perfectly ordered, defect-free, intermetallics, the major contributions to their finite-temperature thermodynamic properties are due to vibrational, electronic, and magnetic degrees of freedom, DOF. Since all the structures examined in this work are nonmagnetic, only vibrational and electronic DOF were taken into account in this work.

1. Vibrational contributions

To calculate the vibrational properties of the structures, the harmonic approximation was used.[27] The frequencies of the 3N independent modes of oscillation (phonons) were determined by diagonalizing the dynamical matrix obtained through the supercell method[13] as implemented in the ATAT package.[28,29]

In this method, the maximum range of the interatomic forces is controlled by the size of the supercell used. In this work, the selected supercells yielded a maximum interaction range of about ~5 Å, encompassing in all cases *at least* the third coordination shell. This criterion guaranteed that the ratio between the shortest and the longest-ranged force constants in all of the structures was less than or equal to ~1/10. The fast convergence in the calculated force constants suggests in turn that the dominant interactions, relevant to the vibrational properties, within all the structures studied are relatively short ranged.

From the phonon density of states, DOS, the harmonic vibrational free energy—per atom—can be calculated through (Ref. 27):

$$F_{vib}(T) = k_B T \int_0^{\infty} \ln\left[2\sinh\left(\frac{h\nu}{2k_B T}\right)\right] g(\nu)\,d\nu, \qquad (1)$$

where k_B is Boltzmann's constant, h Planck's constant, T the temperature, and $g(\nu)$ the phonon density of states of the structure, normalized to three per atom.

The vibrational properties of the structures can alternatively be characterized by their Debye temperatures, Θ_D, which can be calculated, for example, by equating the nth moment of the corresponding $g(\nu)$ to that of a Debye spectrum, with ν_D being the cutoff frequency (Ref. 30):

$$\theta_D(n) = \frac{h}{k_B}\left[\tfrac{1}{9}(n+3)\int_0^{\nu_{\max}} \nu^n g(\nu)^* d\nu\right]^{1/n} \quad (n>-3, n\neq 0),$$

$$\theta_D(0) = \frac{h}{k_B}\exp\left\{\tfrac{1}{3}\left[1+\int_0^{\nu_{\max}} \ln(\nu) g(\nu)^* d\nu\right]\right\} \quad (n=0). \qquad (2)$$

In a Debye solid, all $\Theta_D(n)$ converge to the same value, Θ_D. In a real crystal, however, the different $\Theta_D(n)$ may be significantly different. In fact, different $\Theta_D(n)$ may be related to different thermodynamic properties. For example, $\Theta_D(0)$ corresponds to the Debye temperature obtained by fitting the entropy of a real solid—up to $\sim\Theta_D$—to the entropy of a Debye solid, in the high-temperature limit. $\Theta_D(2)$ in turn corresponds to the "specific heat" Debye temperature. Even $\Theta_D(-2)$ has an important physical meaning as it is related to the root-mean-square amplitude of thermal oscillations according to the Debye-Waller theory.[31,32]

Using $\Theta_D(0)$ as the characteristic harmonic Debye temperature, one can in turn approximate, in the high-temperature limit, the vibrational free energy—per atom—of a structure (Ref. 33):

$$F_{vib}(T) = \frac{9}{8}k_B\Theta_D - 3k_B T\left[\frac{1}{3} + \ln\left(\frac{T}{\Theta_D(0)}\right) + \cdots\right], \qquad (3)$$

where $\frac{9}{8}k_B\Theta_D$ corresponds to the zero-point vibrational energy.

2. Quasiharmonic corrections

As temperature increases, the amplitude of ionic oscillations do so accordingly, making the vibrational behavior of the crystal increasingly anharmonic. The resulting volume expansion can, to a first approximation,[34] be taken into account through the so-called quasiharmonic correction.[27,35] In this approach the force-constant tensors of the crystal are assumed volume-dependent, resulting in a volume dependence of the phonon DOS. In practice, the quasiharmonic correction is implemented by performing harmonic calculations at several volumes, yielding a vibrational free energy surface spanning the $[V,T]$ space. In this work, five volumes were considered for each structure, with a maximum volume expansion of $\sim 10\%$.

Lattice anharmonicity *due to volume expansion* can be characterized through the mode Grüneisen parameter, $\gamma_i = -\partial \ln \nu_i / \partial \ln V$. When all γ_i are equal, γ_i coincides with the thermodynamic Grüneisen parameter[36] (Section 5.2):

$$\gamma_{\text{th}} = \frac{\alpha_V V B_T}{C_V}, \tag{4}$$

where α_V is the volume coefficient of thermal expansion (CTE), B_T the isothermal bulk modulus, and C_V the heat capacity at constant volume.

The quasiharmonic effects can also be calculated through the change in Θ_D with volume (Ref. 37):

$$\gamma = -\partial \ln \theta_D / \partial \ln V \tag{5}$$

Provided there are no high-order anharmonic effects, the particular choice of $\Theta_D(n)$ in Eq. (5) is not important.[38] In the high-temperature limit one can calculate the quasiharmonic contributions—per atom—to the free energy through (Ref. 27):

$$F(T)_{vib,qh} \sim -\frac{(3k_B T\gamma)^2}{2B_T(V_0/N)}, \tag{6}$$

where V_0 is the equilibrium volume. In a quasiharmonic solid, at $T \geqslant \Theta_D$ the harmonic DOF have already been fully excited and any increase in vibrational disorder—i.e., entropy—is due to the increase in DOF available due to volume expansion. Thus, any two phases with similar harmonic entropies at $T \sim \Theta_D$ but different thermal expansion will have increasingly different entropies as $T > \Theta_D$. However, the increase in vibrational disorder is partly cancelled out—by half in truly quasiharmonic solids—due to a corresponding increase in the static energy as volume increases.[27,39]

3. Electronic contributions

In this work, the contributions—in metallic structures—due to electron disorder at the Fermi level, ε_F, were calculated within the one-electron approximation.[40] In this approximation, the energy—per atom—of the electrons close to ε_F is given by:

$$E_{el}(V,T) = \int n(\varepsilon,V) f \varepsilon d\varepsilon - \int^{\varepsilon_F} n(\varepsilon,V)\varepsilon d\varepsilon, \tag{7}$$

where $n(\varepsilon,V)$ is the electronic DOS and f is the Fermi function. The electronic entropy, S_{el}, is in turn calculated through:

$$S_{el}(V,T) = -k_B \int n(\varepsilon,V)[f \ln f + (1-f)\ln(1-f)]d\varepsilon. \tag{8}$$

The effects of volume on the TEC were also taken into account, yielding a volume-dependent electronic free energy, $F_{el}(V) = E_{el}(V) - TS_{el}(V)$. In Eq. (7) and Eq. (8), the Fermi distribution f needs to be calculated self-consistently, requiring the determination of ε_F at each temperature. As a time-saving measure, the electronic free energy *at each volume* was calculated at only three different temperatures and then fitted to the expression (Ref. 39):

$$F_{el} = -\frac{1}{2}C_{el}T^2 + O\left[\left(\frac{k_B T}{\varepsilon_F}\right)^3\right], \tag{9}$$

where C_{el} corresponds to the linear coefficient of the low-temperature heat capacity, neglecting mass enhancement due to electron-phonon interactions. C_{el} can be alternatively approximated using (Ref. 41):

$$C_{el} \sim \frac{1}{3}\pi^2 n(\varepsilon_F, V_0) k_B^2 T. \tag{10}$$

Using Eq. (6) and Eq. (10), the ratio of electronic to quasiharmonic contributions to the total free energy, η, can be estimated through:

$$\eta = \frac{\pi^2}{27}\frac{B_T(V_0/N)(n(\varepsilon_F,V_0)/N)}{\gamma^2}. \tag{11}$$

4. Total free energy

The vibrational and electronic free energies were calculated directly through Eq. (1), Eq. (7), and Eq. (8) at *each of the volumes* considered for each structure, at 1 K intervals. The cold energy curve at 0 K was then added to these calculations to obtain the total free energy. At each temperature, the free energy was fitted to an equation of state of the form (Ref. 42):

$$F_{Tot}(V) = a + bV^{-1/3} + cV^{-2/3} + dV^{-1}. \tag{12}$$

Through the fitting procedure, the zero-pressure free energy—as well as the volume, bulk modulus, and bulk modulus pressure derivative—were obtained[42] as a function of temperature. By extracting the zero-pressure free energy, the thermochemical properties—such as enthalpy, entropy, and specific heat—were also obtained.

III. PROPERTIES AT 0 K

The structures of the Mg-Ca-Sn ternary are enumerated in Table I. The Ca-Sn binary[12] has seven stable compounds located mostly in the central compositions of the phase diagram. The relative abundance of intermetallic phases suggest, in this case, strong interactions between Ca and Sn. The other two binaries, Mg-Ca (Ref. 15), and Mg-Sn (Ref. 16) are dominated instead by just one central compound with the Mg_2X stoichiometry. One would therefore expect less strong binding energies between Mg and either Ca or Sn and as a

TABLE I. Calculated and experimental lattice parameters, in Å.

Compound	S. G.	a			b			c			Ref.
		GGA	LDA	Exp[a]	GGA	LDA	Exp[a]	GGA	LDA	Exp[a]	
Ca	$Fm\bar{3}m$	5.52	5.33	5.59							67
Mg	$P6_3/mmc$	3.18	3.12	3.21				5.22	5.12	5.21	67
Sn	$I4_1/amd$	5.93	5.79	5.83				3.23	3.13	3.18	67
Ca_2Sn	$Pnma$	7.79	7.04	7.99	5.13	5.19	5.04	9.59	9.26	9.56	12
Ca_5Sn_3	$I4/mcm$	8.15	7.96	8.12				15.48	14.92	15.43	12
$Ca_{36}Sn_{23}$	$P4/mbm$	12.52	12.19	12.50				23.18	22.56	22.88	12
$Ca_{31}Sn_{20}$	$I4/mcm$	12.55	12.23	12.52				40.08	38.88	39.87	12
Ca_7Sn_6	$Pnma$	7.93	7.74	7.87	23.88	23.19	23.83	8.50	8.25	8.46	12
CaSn	$Cmcm$	4.82	4.67	4.81	11.63	11.32	11.54	4.39	4.28	4.35	12
$CaSn_3$	$Pm\bar{3}m$	4.78	4.64	4.74							12
Mg_2Sn	$Fm\bar{3}m$	6.82	6.68	6.76							12
Mg_2Ca	$P6_3/mmc$	6.23	6.09	6.23				10.07	9.84	10.10	67
MgCaSn	$Pnma$	7.88	7.67	7.87	4.72	4.61	4.69	8.82	8.60	8.75	68
$Mg_{3.8}Ca_{6.2}Sn_7$[b]	$Pbam$	7.84	7.62	7.79	25.97	25.31	25.72	4.70	4.59	4.66	69

[a] The experimental lattice parameters are reported at room temperature.

[b] This compound exhibits disorder in one crystal position (Ref. 69), which has the Mg1/Ca4 composition. To model this, a supercell was used.

result the Mg_2X compounds would be less stable than the Ca-Sn intermetallics. These observations are confirmed below (see Sec. III D). Within the ternary Gibbs triangle, experiments have only revealed the existence of two intermetallic compounds, located in the central region of the Mg-Ca-Sn composition space.

In this section we present the results of the calculations for the low temperature properties of the intermetallic compounds in the Mg-Ca-Sn ternary system.

A. Lattice parameters

Table I shows that the calculated and experimental lattice parameters for all the known intermetallic compounds in the Mg-Ca-Sn system agree rather well. As it is usually the case in metallic systems, the GGA calculations yield lattice parameters with a better match to experiments (average error of about ~+0.7%) than those obtained through the LDA (average error around ~−2.5%). It is also evident from the table that the lattice parameters calculated with the GGA tend to be larger than those obtained through the LDA due to the overestimation of the binding energies of the latter.

B. Structural properties at 0 K

From the cold energy curve the EOS of the compounds was obtained through Eq. (12) and the procedure described in Shang and Böttger.[42] From the EOS, the structural properties—equilibrium volume, V_0, cohesive energy, E_{coh}, bulk modulus, B_T, and the pressure derivative of the latter, B_T'—for several structures in the Mg-Ca-Sn ternary were calculated. As can be seen in Table II, the calculated and experimental cohesive energies for fcc Ca, hcp Mg, and $\beta-$Sn agree rather well, differing in the worst case by less than 10 meV. Similar agreement is observed in the case of B_T and even of B_T'. Although there is no experimental data to confirm the calculations, we can reasonably infer that the same level of accuracy can be expected for the remaining intermetallics.

C. Electronic structure

Figure 1 shows the electronic DOS, $n(\varepsilon)$, for several structures in the Mg-Ca-Sn ternary system, calculated self-consistently within the GGA. The structures presented in this figure correspond to the compounds for which the vibrational contributions are presented in Sec. II B. The figure clearly indicates definite differences in the bonding character among the different structures: fcc Ca, for example, has the highest electron density at the Fermi level and it is therefore the structure with the highest TEC, as can be seen in Table VI. In fact, only in this structure electronic effects are more dominant than quasiharmonic contributions—see Eq. (11)—due to thermal expansion at $T > \Theta_D$. At the other end of the spectrum, in Ca_2Sn the Fermi energy lies within a relatively wide band gap of about ~1 eV, making this structure semiconducting in character, confirming calculations by Migas *et al.*[64] Obviously, electronic contributions in this case are not existent. Of the remaining structures, Mg_2Sn and MgCaSn are the other structures which have the smallest TEC, as can be seen in Table VI.

D. Enthalpies of formation

Table III shows the calculated GGA and LDA enthalpies of formation for the intermetallic phases in the Mg-Ca-Sn

TABLE II. Structural properties of Mg-Ca-Sn structures at 0 K. The calculations were obtained by fitting the cold energy curve—obtained using the GGA—through Eq. (12) and the expressions derived in Shang and Böttger (Ref. 42). Underlined quantities correspond to experimental measurements.

Structure	V_0/N Å^3	E_0/N eV	E_{coh}/N[a] eV	B_T GPa	B'_T
fcc Ca	42.564	−1.908	−1.900, $\underline{-1.822}$[b]	18.25, $\underline{17}$[e], $\underline{18.3}$[f]	3.60
hcp Mg	22.908	−1.524	−1.484, $\underline{-1.51}$[c]	36.56, $\underline{45}$[e], $\underline{35.2}$[f], $\underline{36.8}$[g]	4.37, $\underline{4.3}$[g]
β Sn	28.386	−3.823	−3.103, $\underline{-3.10/-3.13}$[d]	48.63, $\underline{58}$[e], $\underline{57.9/54.9}$[h]	4.81, $\underline{4.8}$[i]
Ca_2Sn	32.544	−3.230	−2.984	29.80	3.17
Ca_5Sn_3	32.531	−3.308	−3.303	32.58	4.29
CaSn	30.914	−3.553	−3.189	38.95	4.70
CaSn3	27.366	−3.769	−3.227	45.88	4.69
Mg_2Sn	26.428	−2.511	−2.244	40.94	4.35
Mg_2Ca	28.370	−1.781	−1.751	30.54	4.01
MgCaSn	27.465	−3.008	−2.751	41.39	4.20

[a] E_{coh} calculated with respect to isolated, spin-polarized atoms.
[b] Reference 33.
[c] Reference 43.
[d] Reference 44.
[e] Reference 45.
[f] Reference 46.
[g] Reference 47.
[h] Reference 48.
[i] Reference 49.

ternary system, as well as the values obtained via experimental work, CALPHAD assessments[15,16,50] as well as empirical models based on the Miedema approach.[51] For most of the compounds—except for Mg_2Ca and Mg_2Sn—the LDA calculations yielded lower enthalpies of formation than those calculated with the GGA, suggesting a greater stability of the compounds with respect to the constituent elements.

With regard to the Ca-Sn binary, the calculated enthalpies of formation *of the Sn-rich compounds* agree well with the available experiments, and even with the enthalpies calculated using the empirical Miedema approach,[51,52] with their values differing by just a few kJ/mol atom. In this binary system, the most noticeable discrepancy corresponds to the enthalpy of formation for Ca_2Sn. The cause is not completely clear, although it is likely, for starters, that in the direct reaction calorimetry experiments by Kubaschewski and Villa[53] the Ca-rich samples were partially oxidized.[14] The more recent measurements by Min and Sao[54] yield similarly exothermic results. In those experiments, the enthalpies of formation were obtained indirectly, by equilibration with liquid silver. This determination required accurate *a priori* knowledge of the thermochemistry of dissolution of Ca and Sn in Ag. The uncertainties involved in those measurements led to conflicting values for the melting enthalpy of Ca_2Sn, as well as the values for the enthalpy of formation of CaO (Ref. 54). More direct determinations and better control of oxidation are thus needed to resolve the discrepancy.

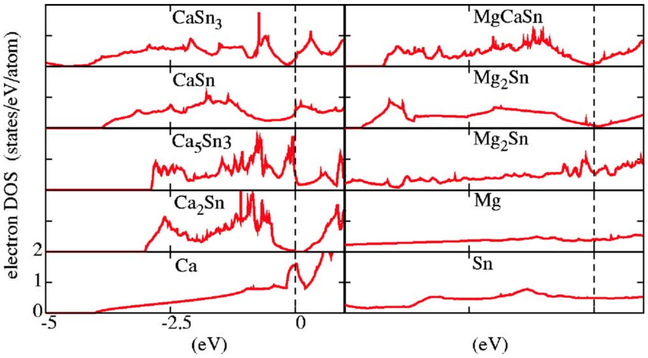

FIG. 1. (Color online) Electronic DOS, $n(\varepsilon)$, for several structures in the Mg-Ca-Sn ternary system. Fermi level is located at 0 eV and is also indicated by dashed lines. All panels were plotted using the same scale.

Table III indicates that the calculated enthalpies of formation for Mg_2Ca and Mg_2Sn binary compounds agree well with all the experimental data available, with differences of less than 3 kJ/mol atom. In the case of Mg_2Sn, the empirical Miedema value[51] is in disagreement with both calculations and experiments, as it underestimates the stability of this phase by almost 100% (−13 kJ/mol atom) on a relative (absolute) basis. Differences of this magnitude are typical of this semiempirical approach.[55]

E. Ground state of Ca-Sn binary

The phase diagram for the Ca-Sn binary[56] accepted until about five years ago contained only four intermetallic phases, namely Ca_2Sn, CaSn, $CaSn_3$, and $Ca_{31}Sn_{20}$. Uncertainties in the liquidus and some invariant temperatures and compositions led Palenzona *et al.*[12] to reinvestigate this system. This recent work resulted in the discovery of three new interme-

TABLE III. Enthalpy of formation ${}^{0}\Delta_{f}H$ (kJ/mol atom) of compounds in Mg-Ca-Sn ternary. Reference states: fcc Ca, hcp Mg, and tetr (β) Sn.

Compound	Exp[a]	CALPHAD	Miedema[b]	GGA[c]	LDA[c]
Ca_2Sn	−104.6±12.6[d], −109.2±0.56[e]		−57.8	−66.0	−70.8
Ca_5Sn_3			−63.6	−65.5	−69.5
$Ca_{36}Sn_{23}$			−65.4	−66.3	−71.0
$Ca_{31}Sn_{20}$			−65.7	−66.4	−70.8
Ca_7Sn_6			−71.4	−65.1	−69.2
CaSn	−79.5±10.5[c], −62.00±1.0[f]		−72.7	−66.0	−70.4
$CaSn_3$	−44.98[c], −38.6[f]		−47.8	−40.9	−45.5
Mg_2Sn	−25.5[e],−23.8[g], −26.8±2.51[h],−24.3±1.260[i]	−26.36[j]	−11.4	−21.3	−21.1
Mg_2Ca	−13.5±0.42[k],−12.7±0.63[l], −13.0±0.88[m]	−13.44[n]	−8.8	−12.3	−12.6
MgCaSn				−56.7	−60.1
$Mg_{3.8}Ca_{6.2}Sn_7$				−56.9	−60.6

[a] The experimental values for the enthalpies of formation are reported at 298 K.
[b] Reference 51.
[c] GGA and LDA results correspond to enthalpies of formation at 0 K. However, the difference with respect to the values at 298 K are expected to be within ∼0.1 kJ/mol atom.
[d] Reference 53.
[e] Reference 71.
[f] Reference 70.
[g] Reference 72.
[h] Reference 73.
[i] Reference 74.
[j] Reference 16.
[k] Reference 75.
[l] Reference 76.
[m] Reference77.
[n] Reference 15.

tallics, Ca_7Sn_6, $Ca_{36}Sn_{23}$, and Ca_5Sn_3 and a substantial modification of the original phase boundaries. The experiments, however, were unable to determine if these three new phases belonged to the ground state of the system.

Figure 2 shows the calculated ground state of the Ca-Sn binary system. In the central region of the composition range, the convex hull is rather flat, with all structures having similar enthalpies of formation. It can also be seen that the ground state, calculated with both the LDA and GGA, consists of the compounds Ca_2Sn, CaSn, and $CaSn_3$, with $Ca_{31}Sn_{20}$ and $Ca_{36}Sn_{23}$ alternatively sitting on the convex hull in the GGA and LDA constructions, respectively—the difference in energies are within the numerical uncertainties of the calculations—confirming the findings by Palenzona *et al.*[12] Figure 2 also shows that Ca_5Sn_3 and Ca_7Sn_6 lie above the convex hull, indicating that these two phases are not stable configurations at 0 K. In the case of Ca_5Sn_3, Palenzona *et al.*[12] suggested that it could have become stabilized due to hydrogen. Its closeness to the ground state makes entropic stabilization a more likely explanation for its presence in the experimental samples. The same argument can be put forward for the case of Ca_7Sn_6.

IV. PROPERTIES AT FINITE TEMPERATURES

Due to limitations in computing resources, calculations of the finite-temperature thermodynamic properties were constrained to fcc Ca, hcp Mg, $\beta-$Sn, Mg_2Ca, Ca_2Sn, CaSn, Ca_5Sn_3, $CaSn_3$, Mg_2Sn, and MgCaSn. Once these crystal structures were optimized, their total free energies were calculated and fitted through Eq. (12). The structures of the

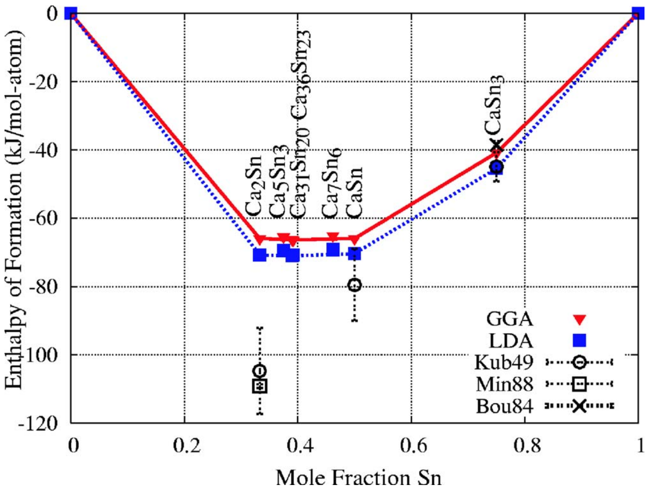

FIG. 2. (Color online) Calculated convex hull of Ca-Sn binary system and comparison with experimental data. The calculated enthalpies of formation are estimated to have a numerical uncertainty of less than 1 kJ/mol atom, smaller than the actual size of the markers. Reference states: fcc Ca and β-Sn.

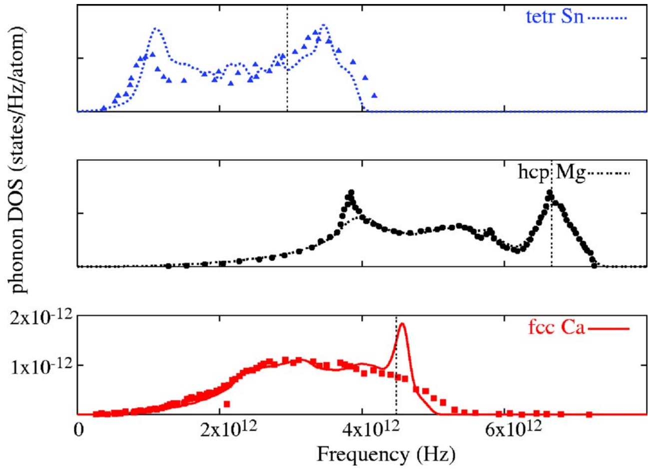

FIG. 3. (Color online) Calculated and experimental (Ref. 30) phonon densities of state for fcc Ca, hcp Mg, and β-Sn. Vertical dashed lines show the location of the Debye frequencies—calculated from $\Theta_D(0)$—for each phonon DOS. All panels were plotted using the same scale.

compounds $Ca_{31}Sn_{20}$, $Ca_{36}Sn_{23}$, Ca_7Sn_6, and $Mg_{3.8}Ca_{6.2}Sn_7$ are rather large, and therefore the calculation of their vibrational properties were deemed prohibitively expensive. For the structures considered in this work, the GGA was used, since it yielded, in general, the best agreement with the experimental lattice parameters.

A. Vibrational properties of Mg-Ca-Sn intermetallics

Figure 3 shows the calculated and experimental phonon DOS for the elemental constituents of the system. For fcc Ca, the agreement between experiments and calculations is very good in the low-frequency region of the DOS. Given that the thermodynamic properties at moderate temperatures are dominated by low frequency modes, one can expect—and it will be shown below—that the thermochemical properties of this structure can be calculated rather accurately. For hcp Mg, there is almost complete point-by-point agreement between experiments and calculations, the only difference being the relative height of the two main peaks of the spectrum. In the case of β-Sn, although the average properties of the calculated and experimental phonon DOS seem to be quite close, there are some noticeable differences, particularly in the low frequency regions. The disagreement in this case may be due to longer-ranged nearest-neighbor interactions in β-Sn that could not be taken into account with the supercell.

The characteristic frequencies of the spectra in Fig. 3 are related to the structural properties (Table II) through (Ref. 33):

$$\nu_D \propto \sqrt{\frac{rB_T}{M}}, \tag{13}$$

where r is the effective interatomic distance $(r \sim (V_0)^{1/3})$ and M is the effective mass of the structure. By using the calculated values for B_T and r, the sequence $\nu_{D,Mg} > \nu_{D,Ca} > \nu_{D,Sn}$ seen in Fig. 3, is recovered, as expected. At high temperatures and using the Debye approximation, the harmonic vibrational entropy can be calculated (Ref. 33):

$$S_{vib} = 3k_B\left[\frac{4}{3} + \ln\frac{k_BT}{h\nu_D} + \cdots\right]. \tag{14}$$

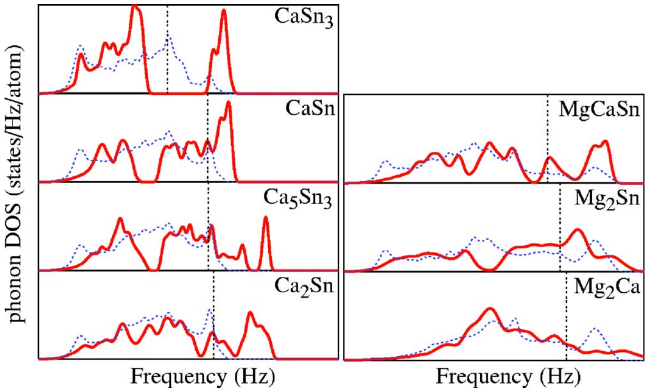

FIG. 4. (Color online) Phonon DOS of intermetallic compounds in the Mg-Ca-Sn system (solid lines). Dashed lines show the composition-weighted average phonon DOS obtained from the calculations for fcc Ca, hcp Mg, and β-Sn. Vertical dashed lines show the location of the Debye frequencies—calculated from $\Theta_D(0)$—for each phonon DOS.

Thus, the structure with the lowest entropy is the one with the highest ν_D and vice versa. These trends are confirmed below in Table VI.

Figure 4 shows the calculated phonon DOS of the compounds studied in this work. Dashed lines correspond to the composition-weighted average phonon DOS of the constituent elements. As can be seen in Fig. 4, in all cases, the difference between the phonon DOS of the compounds and the average of the constituents, $\Delta g(\nu)$, *at low frequencies* is negative. The compounds' phonon spectra are shifted toward higher frequencies, indicating a stiffening of the interatomic bonds upon compound formation. The smaller atomic volumes of the compounds as compared to the weighted-average volume of their constituents (see Table II) are also consistent with the observed bond stiffening. Since $\Delta S_{vib} = k_B \int \ln\left(\frac{k_BT}{h\nu}\right)\Delta g(\nu)d\nu$ (Ref. 39), a shift to higher frequencies—negative $\Delta g(\nu)$—results in negative entropies of formation, as indicated in Table VII. The accessible vibrational DOF are therefore decreased upon alloying.

By observing the area enclosed between the two phonon DOS for each structure, as well as the calculated enthalpies of formation—see Table III—it is also evident that a larger area—larger accumulated $\Delta g(\nu)$ in the low frequency region—is associated with a higher stability—more negative $^0\Delta_f H$. For example, the smallest accumulated $\Delta g(\nu)$ corresponds to the phonon DOS of Mg_2Ca, which is in turn the compound with the least negative enthalpy of formation, according to Table III, suggesting a relationship between the stability of a compound and the vibrational entropy reduction upon compound formation.

Figure 4 also shows that, to a first approximation, the center of mass, as well as the width of the phonon spectra for

TABLE IV. Vibrational properties of Mg-Ca-Sn intermetallics: Debye frequency, ν_D; average frequency, $\langle \nu \rangle$; maximum frequency, ν_{max} as well as Debye temperatures, $\Theta_D(n)$ derived from the nth moment (Ref. 30) of the phonon DOS—see Table III and Fig. 4. Results correspond to GGA calculations.

Compound	ν_D[a] THz	$\frac{\langle \nu \rangle}{\nu_{max}}$	ν_{max} THz	$\Theta_D(0)$[b]	$\Theta_D(2)$[b]	$\Theta_D(4)$ K	$\Theta_D(-2)$[b]
fcc Ca	4.48	0.65	5.17	215.10	216.49, 218[c]	218.97	227.98
hcp Mg	6.66	0.66	7.51	319.73	320.49, 323[c]	323.94	344.63
β Sn	2.95	0.57	4.14	141.67	156.93, 166[c]	166.05	148.84
Ca_2Sn	4.66	0.58	6.40	223.58	245.70	260.68	225.12
Ca_5Sn_3	4.53	0.56	6.32	217.61	236.28	249.85	226.89
CaSn	4.51	0.65	5.42	216.48	232.38	240.24	215.83
$CaSn_3$	3.44	0.52	5.36	165.32	189.58	210.95	180.36
Mg_2Sn	5.77	0.57	8.14	276.75	307.96	321.07	258.82, 270 ± 3[d]
Mg_2Ca	5.94	0.53	8.52	285.25	290.89	301.49	331.31
MgCaSn	5.44	0.58	7.40	260.99	286.63	305.02	266.11

[a] Debye frequency, ν_D calculated using $\Theta_D(0)$.
[b] See text for the definitions of these $\Theta_D(n)$.
[c] Reference 30.
[d] Reference 31.

all the compounds are similar to those of the corresponding weighted-averaged phonon DOS. Thus, the compounds' phonon DOS seem to be determined in great part by the identities of their constituent elements, while symmetry and changes in the electronic structure determine finer details of the respective spectra, such as band gaps, discontinuities, and so forth. The relatively small vibrational entropies of formation, relative to the absolute entropies of the products and reactants, is a direct consequence of this.

Table IV shows a summary of the vibrational properties of the structures in the Mg-Ca-Sn system. The experimental Debye temperatures for fcc Ca, hcp Mg, and β-Sn correspond to the "heat capacity" Debye temperature, which can be approximated at high temperatures through $\Theta_D(2)$. Table IV shows that there is good agreement between experiments and calculations for fcc Ca and hcp Mg, with differences within a few K. For β-Sn, the difference is higher (about ~7 K), with calculations suggesting a softer structure—lower Θ_D—implying an overestimation of the entropy of β-Sn, as shown below. In the case of Mg_2Sn, the discrepancy between the calculated and experimental[31] $\Theta_D(-2)$ is somewhat larger, albeit still within ~10 K.

As can be seen in the Table IV, the differences among the $\Theta_D(n)$ is almost negligible for some structures (fcc Ca and hcp Mg) while in others this difference amounts to almost 60 K ($CaSn_3$). The degree of variation in the $\Theta_D(n)$ for a particular structure indicates how far/close its vibrational spectrum is from that of a Debye solid. Thus, large differences among $\Theta_D(0)$, $\Theta_D(2)$, and $\Theta_D(4)$ indicate the presence of band gaps and higher-than-quadratic frequency dependence of the phonon DOS, such as is the case of $CaSn_3$.

B. The effects of lattice expansion

As mentioned in Sec. II B 2, the effects of volume expansion can be taken into account through the quasiharmonic correction. Since volume changes in the quasiharmonic approximation only tend to shift the frequencies of the phonon DOS but not in its shape, the particular choice of the nth moment does not make a noticeable difference. In this work, the change of the zeroth moment $\Theta_D(0)$ with volume was used to obtain γ.

Table V presents the experimental and calculated Grüneisen parameters for several structures. γ can also be calculated, within the mean-field approximation, through (Ref. 57):

$$\gamma = \frac{1}{2}\left(B'_T - \frac{1+2\lambda}{3}\right), \tag{15}$$

where the parameter λ assumes the value of 0, 1, or 2 depending on whether Slater's,[58] Dugdale-MacDonald's[59] or Vashchenko-Zubarev's[60] approximations were used. Respectively, these three approximations assume no volume dependence of the Poisson ratio; simple harmonic lattice; and 3D anharmonic oscillators. The table indicates that the Grüneisen parameters calculated directly from the changes in the phonon DOS, $\gamma_{\Theta D}$—rather than the γ's from the cold energy curve—agreed consistently better with the experimental values.

Assuming that $\gamma_{\Theta D}$ is correct, inspection of the table also indicates that the approximation due to Dugdale and MacDonald[59] is slightly more consistent than the other two mean-field approaches at predicting γ. However, no definitive statement can be made regarding the ability of either theory to correctly predict anharmonic effects. It can also be observed that despite the wide variability, there is an overall tendency for the structures with the greater B'_T, shown in Table II, to have the greater γ and therefore the greater contribution from thermal expansion to the free energy, which is

TABLE V. Grüneisen constants for intermetallic compounds in the Mg-Ca-Sn ternary system. Effects due to TEC have been excluded in order to properly characterize and quantify only quasiharmonic effects. Calculations indicate that temperature dependence is almost linear up to the melting point.

Compound	γ_{Θ_D}		$\gamma_{\lambda=0}$[a]		$\gamma_{\lambda=1}$[a]		$\gamma_{\lambda=2}$[a]		γ_{exp}
	0 K	298 K	0 K	298 K	0 K	298 K	0 K	298 K	
fcc Ca	1.16	1.21	1.64	1.67	1.31	1.33	0.97	1.00	1.07[b,d]
hcpMg	1.59	1.66	2.05	2.10	1.71	1.77	1.38	1.43	1.69[c,e]
β Sn	2.19	2.36	2.25	2.33	1.92	2.00	1.59	1.66	2.55[c,e]
Ca_2Sn	1.20	1.28	1.42	1.44	1.09	1.11	0.76	0.77	
Ca_5Sn_3	1.38	1.42	1.99	2.03	1.66	1.69	1.32	1.36	
CaSn	1.55	1.58	2.20	2.25	1.86	1.91	1.53	1.58	
$CaSn_3$	2.15	2.40	2.19	2.28	1.86	1.94	1.53	1.61	
Mg_2Sn	1.51	1.53	2.02	2.05	1.69	1.73	1.36	1.39	~1[f]
Mg_2Ca	1.44	1.51	1.86	1.90	1.52	1.56	1.19	1.23	
MgCaSn	1.47	1.52	1.95	1.98	1.61	1.65	1.28	1.31	

[a] These Grüneisen constants were calculated using the cold curve at zero pressure through (Ref. 57): $\gamma = \frac{1}{2}\left(B'_T - \frac{1+2\lambda}{3}\right)$. $\lambda = 0$, 1 and 2 corresponds to the derivations by Slater (Ref. 58), Dugdale and MacDonald (Ref. 59), and Vashchenko and Zubarev (Ref. 60), respectively.

[b] Experimental Grüneisen constant at 0 K.

[c] These Grüneisen constants are reported at 300 K.

[d] Reference 33.

[e] Reference 57.

[f] Reference 78.

consistent with Eq. (15). The weak positive temperature dependence of γ, along with Eq. (10) and Eq. (6) also suggests,as shown in Fig. 5(c) and Fig. 6, a rather linear increase of the specific heat as a function of temperature.

C. Thermodynamics at finite temperatures

As a benchmark for the supercell method used in this work, and to illustrate the relative contributions of the different DOF to the total free energy, the calculated enthalpy, entropy, and specific heat for hcp Mg are compared to the tabulated data by Barin [61] in Fig. 5. In the figures, four different curves can be seen. The one labeled *h* corresponds to the *harmonic* free energy. The curve labeled as $h+el$ incorporates the TEC. The effects of lattice expansion on the harmonic free energy are shown in the curve labeled as *qh*. Finally all contributions are taken to account in the curve labeled as $qh+el$.[62]

Figure 5 shows that only through the consideration of *all* contributions to the total free energy it is possible to accurately reproduce the experimental data. It can also be seen that the calculated specific heat shows a worse agreement with experiments, due to the fact that this quantity—being a second derivative of the free energy—is very sensitive to changes in the curvature of the enthalpy/entropy curves. Figure 5 also shows that, for this structure, electronic contributions are not as important and vibrational ones. This is due to the relatively low electron DOS at the Fermi level, ε_F. This low DOS at ε_F was also observed in almost all the other structures calculated in this work.

Table VI shows that the calculated and experimental entropies agree within a few J/mol/K for most of the structures, with Ca_2Sn and CaSn being the sole exceptions. In these cases, the discrepancy is likely due to integration errors in the extrapolations from high-temperature experimental heat capacity and enthalpy data.[63] For the C_P, the calculations for all the structures agree within 1 J/mol/K, except for β-Sn, in which the calculated C_P overestimates the experimental data by almost 4 J/mol/K. This is consistent with the underestimation of the Debye temperature, $\Theta_D(2)$, shown in Table IV.

Table VI also shows that the calculated isotropic linear thermal expansion coefficient, α_L, agrees reasonably well with the measurements at room temperature. This agreement, however, is not expected to hold at higher temperatures as higher-order anharmonic effects not taken into account in the quasiharmonic approximation start to become important.[43]

In Sec. II, η—Eq. (11)—was defined as the ratio between the electronic and quasiharmonic contributions to the total free energy of the structures. Table VI shows that in only one case (fcc Ca), electronic contributions are dominant. This structure has the highest linear coefficient for the electronic heat capacity, C_{el} in Eq. (10), which compares well with the available experimental data. Since the Fermi level in Ca_2Sn lies within a band gap—in agreement with Migas *et al.*[64]—there are no TEC to the total free energy. Mg_2Sn is another compound for which its TEC are negligible.[65]

The thermodynamic properties of fcc Ca, β-Sn, CaSn, and Mg_2Ca, and their comparison with the available experimental/tabulated data are presented in Fig. 6.[66] In these four cases, the calculated enthalpies and specific heats agree very well with the tabulated data. The biggest discrepancy corresponds to the entropy of CaSn, which, as mentioned above, may be due to erroneous extrapolations from high-temperature data.[63]

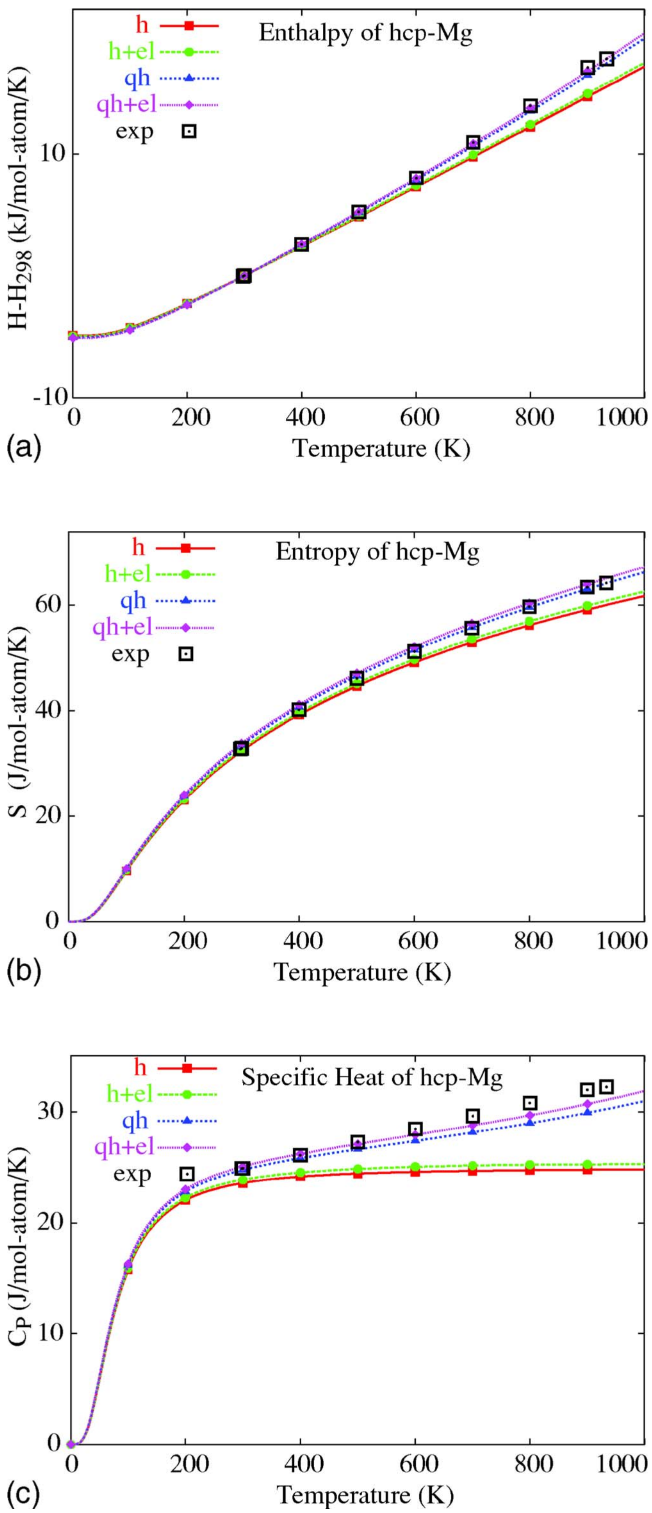

FIG. 5. (Color online) Thermodynamic properties of hcp Mg. Experimental thermodynamic (Ref. 61) data are presented for comparison. Results depict four curves: *h* includes only harmonic contributions; *h+el* incorporates electronic DOF; *qh* corresponds to the quasiharmonic correction without TEC and finally, *qh+el* corresponds to calculations that include *all* contributions to the total free energy. Higher-order anharmonic effects due to phonon-phonon and electron-phonon couplings, as well as the effect of thermal defects are not included.

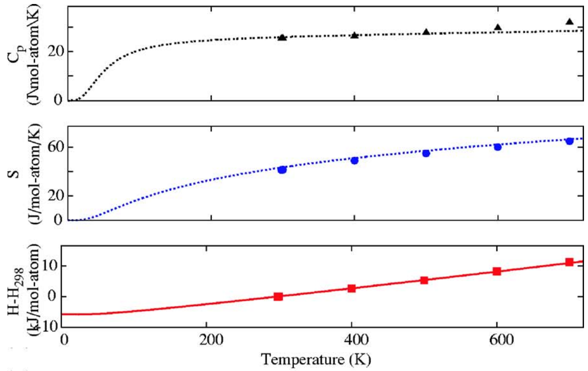

(a)

Thermochemical Properties of fcc Ca

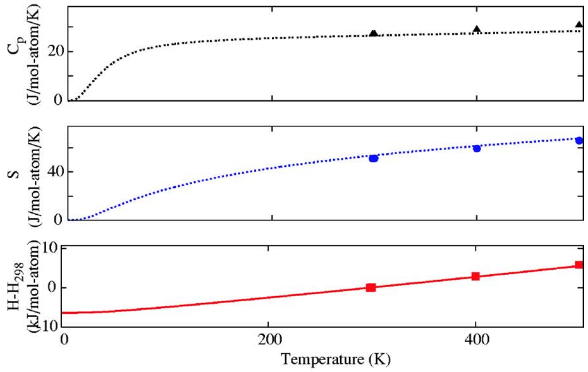

(b)

Thermochemical Properties of β Sn

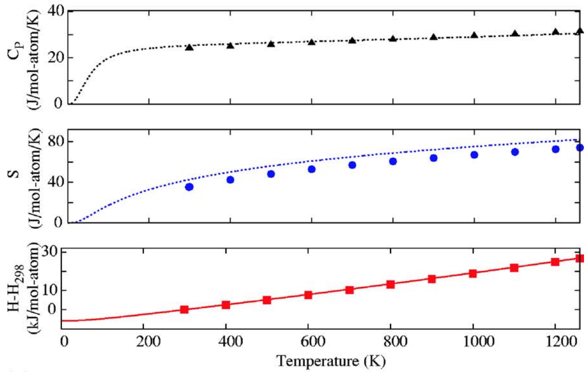

(c)

Thermochemical Properties of CaSn

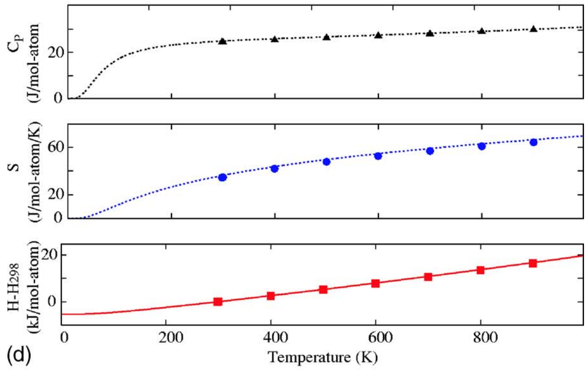

(d)

Thermochemical properties of Mg_2 Ca

FIG. 6. (Color online) Calculated and experimental (Ref. 61) enthalpies, entropies, and specific heat for fcc Ca, β-Sn, CaSn, and Mg_2Ca.

TABLE VI. Thermodynamic properties of intermetallic compounds in the Mg-Ca-Sn ternary system. Underlined quantities correspond to experimental data. A reduction of the specific heat to a simple algebraic expression is given in the Appendix .

Compound	S_{298}[a] J/mol/K	$C_{P,298}$[a] J/mol/K	$\alpha_{L,298}$[b] 1×10^{-6} 1/K	$B_{T,298}$ GPa	dB_T/dT_{298}[c] $\times10^{-3}$ GPa/K	η[d]	C_{el}[d] mJ/atom/K^2
fcc Ca	43.36, $\underline{41.42}$	25.89, $\underline{25.31}$	22.78, $\underline{22.3}$[e]	16.94	−4.25	2.06	3.83, $\underline{2.9}$[f]
hcp Mg	33.55, $\underline{32.68}$	25.05, $\underline{24.9}$	29.51, $\underline{26.0}$[g]	32.34	−13.33, $\underline{-20.8}$[h,i]	0.30	0.9, $\underline{1.3}$[f]
β Sn	53.77, $\underline{51.20}$	26.22, $\underline{30.73}$	26.70, $\underline{22}$[g]	43.38	−17.69	0.32	1.2, $\underline{1.78}$[f]
Ca_2Sn	41.40, $\underline{33.47}$	24.78, $\underline{23.87}$	20.23	28.07	−5.55	0	0
Ca_5Sn_3	42.50	25.17	19.47	30.22	−7.60	0.68	1.55
CaSn	42.64, $\underline{35.36}$	24.06, $\underline{25.28}$	19.05	35.86	−10.00	0.59	1.28
$CaSn_3$	50.01	26.58	31.51	40.24	−19.09	0.15	0.57
Mg_2Sn	36.47, $\underline{34.3}$[j]	24.45, $\underline{24.44}$[j]	19.66	37.69	−10.14	0.09	0.15, $\underline{0.08}$[j]
Mg_2Ca	36.21 $\underline{34.6}$	25.20, $\underline{24.58}$	25.72	27.71	−9.00	0.52	1.35
MgCaSn	37.83	24.62	19.41	38.31	−9.7	0.08	0.11

[a] Experimental data for S and C_P obtained from Barin (Ref. 61) unless otherwise noted.
[b] $\alpha_{L,298}$ is the isotropic linear thermal expansion coefficient.
[c] The value for dB_T/dT_{298} was obtained in Ref. 47 through fitting of P-V-T data to a Birch-Murnaghan EOS.
[d] η represents the ratio of electronic to quasiharmonic contributions.
[e] Reference 45.
[f] Reference 41.
[g] Reference 79.
[h] Reference 47.
[i] The linear coefficient of the electronic heat capacity was calculated directly from a linear fitting of the calculations and incorporates volume expansion effects.
[j] Reference 65.

D. Formation properties of the compounds

Table VII shows the formation properties, ${}^0\Delta_f H$ and ${}^0\Delta_f S$, of the Mg-Ca-Sn compounds at 298 K. In all cases, ${}^0\Delta_S H_{298}$ is negative. It can also be seen that the most important contribution to the entropy difference is the *decrease* in the harmonic vibrational entropy due to bond stiffening upon compound formation. The table also shows that electronic and volume expansion effects contribute, at 298 K, with only a fraction of the total entropies of formation. On absolute terms, these contributions are within the 0.1–1 J/mol atom/K range. On relative terms, these nonharmonic contributions to the enthalpy of formation are even less significant. As temperature increases, these nonharmonic contributions increase in importance since at temperatures beyond Θ_D—according to Table IV in all cases Θ_D is less or

TABLE VII. Formation properties, at 298 K for intermetallic compounds in the Mg-Ca-Sn ternary system.

Compound	${}^0\Delta_f H_{298}$ kJ/mol-atom	$\frac{d\Delta_f H}{dT}$ kJ/mol-atom/K 1×10^{-3}	$\frac{d\Delta H^{el}}{d\Delta H^{qh}}$[a]	${}^0\Delta_f S_{298}$ J/mol-atom/K	$\frac{{}^0\Delta_f S^{el}_{298}}{{}^0\Delta_f S^{h}_{298}}$[b] %	$\frac{{}^0\Delta_f S^{qh}_{298}}{{}^0\Delta_f S^{h}_{298}}$[c] %	$\frac{d\Delta_f S}{dT}$ J/mol atom/K^2 1×10^{-3}
Ca_2Sn	−66.1	−1.52	+1.93	−5.40	19	5	−3.83
Ca_5Sn_3	−65.80	−1.08	+0.84	−4.07	9	7	−2.72
CaSn	−66.34	−0.99	+0.64	−5.23	6	6	−2.49
$CaSn_3$	−40.89	+0.56	−0.45[d]	−1.30	25	−41	+1.37
Mg_2Sn	−21.30	−1.30	+0.47	−3.01	8	17	−3.26
Mg_2Ca	−12.44	−0.05	−0.46[e]	−0.46	25	12	−0.14
MgCaSn	−56.89	−1.36	+0.98	−4.84	10	7	−3.43

[a] This ratio is almost identical to $\frac{d\Delta S^{el}}{d\Delta S^{qh}}$.
[b] Percentage of the entropy of formation due to thermal electronic contributions, at 298 K.
[c] Percentage of the entropy of formation due to thermal expansion anharmonic effects, at 298 K.
[d] Note that in this case, quasiharmonic effects actually stabilize the structure at higher temperatures, therefore $d\Delta_f H^{qh}/dT$ and $d\Delta_f S^{qh}/dT$ have *positive* signs.
[e] In this case, $d\Delta_f H^{el}/dT$ and $d\Delta_f S^{el}/dT$ are the ones with *positive* signs.

close to 298 K—the harmonic entropy and enthalpy of formation are essentially constant.

The table also indicates that in all cases the electronic entropy of formation is always negative. As can be seen in Fig. 1, upon compound formation, the electron DOS at the Fermi level decreases (in some cases—i.e., Ca_2Sn—it disappears completely) relative to that of the constituent elements, therefore *reducing* the degree of electronic disorder. Likewise, the net reduction in the number of thermal electrons reduces the electronic enthalpy, relative to the constituent elements. However, the changes in the electronic enthalpy are, according to Eq. (9), only half those of the entropy.

In the majority of the structures, except for $CaSn_3$, it is also found that the quasiharmonic entropies of formation are negative. By examining Table VI it can be seen that in most cases the linear thermal expansion coefficients, α_L, are smaller than the weighted average of the constituent elements. The smaller rate of volume expansion leads to a slower rate of increase of the accessible vibrational DOF, relative to the constituent elements. This is not the case for $CaSn_3$, and as can be seen in Table VII, quasiharmonic contributions actually make entropy of formation *less* negative—by -41%.

By comparing the values of the enthalpies and entropies of formation for $CaSn_3$, Mg_2Sn, and Mg_2Ca to those of Ca_2Sn, Table VII also suggests a (weak) correlation between the enthalpies and entropies of formation of the compounds. This is to be expected since a more negative enthalpy of formation is an indicator of a greater stability and stronger interatomic bonding. Stronger bonding leads to lower vibrational and electronic entropies, leading to a *more* negative entropy of formation for the compounds, relative to their constituent elements.

Interestingly, Table VII also suggests that, contrary to what is observed in the case of the absolute thermodynamic properties (see η in Table VI), *differences* in the TEC tend to have a more significant contribution to the formation properties of the compounds than those due to differences in the rates of volume expansion. The reason for this is that in the majority of the cases, the *decrease* in the electron density at ε_F is more abrupt than a *reduced* softening rate of the compounds compared to their constituent elements. This essentially shows that it is not possible to neglect TEC when studying the formation thermodynamic properties of intermetallics. Of all the compounds studied, only in Mg_2Sn, quasiharmonic contributions are significantly more important than electronic ones.

The table also shows that the temperature dependence of the formation properties is negative in the majority of the cases. For Ca_2Sn, electronic effects have twice the influence of quasiharmonic contributions on this temperature dependence. In the case of $CaSn_3$, the trend is reversed, with quasiharmonic effects being twice as important as the electronic ones in determining $d\Delta_f H/dT$ and $d\Delta_f S/dT$. In the case of the electronic enthalpies and entropies of formation, their negative temperature dependence can be attributed to a increased difference between the electron disorder of the constituent elements and the compounds as temperature increases. The negative slope of the quasiharmonic formation properties is due to the fact that the compounds, except for $CaSn_3$, soften at a slower rate than the constituent elements as the temperature increases. The differences in the rate of softening illustrated in Fig. 7 can be compared to Table VII. In the figure it can be seen that $CaSn_3$ is the structure with the largest dB_T/dT and is also the one with *positive* $d\Delta_f H/dT$ and $d\Delta_f S/dT$.

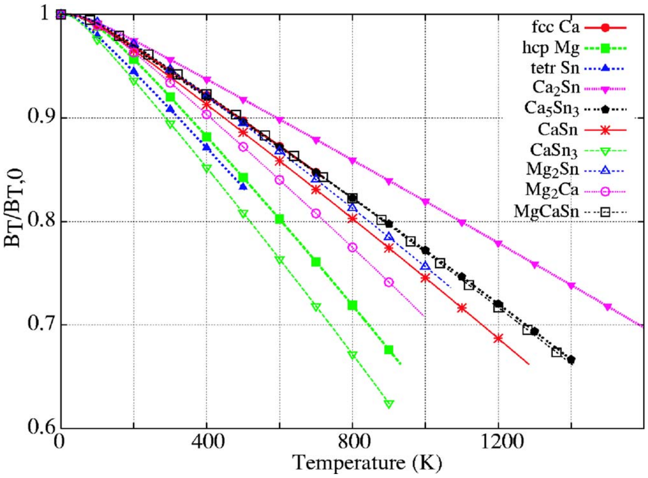

FIG. 7. (Color online) Temperature dependency of the relative bulk modulus ($B_T/B_{T,0}$) for several structures in the Mg-Ca-Sn system.

Table VII shows additionally that the calculated temperature dependence of the enthalpies and entropies of formation are not important and in fact partially cancel each other. For example, an increase in T of 500 K would lead to a *decrease* in the entropy of formation—~ -2 J/mol atom/K at the most. However, the corresponding increase in the free energy of formation is attenuated by a decrease in the enthalpy of formation—$\sim +1$ kJ/mol atom—, yielding a total positive change in the free energy of formation of just $\sim +0.5$ kJ/mol atom for Ca_2Sn, which is the structure with the greatest temperature effects on the enthalpies and entropies of formation. Thus, the net result of quasiharmonic and electronic contributions is to make the structures, except for $CaSn_3$, less stable than their constituent elements. The change in the stability is, however, rather small (in the order of 1 kJ/mol atom). Despite this, the effect on the actual temperature range for the stability of the structures could still be within the ~ 100 K range.

V. CONCLUSION

In this work, a comprehensive analysis of the structural, electronic, and vibrational properties of the intermetallic compounds in a ternary system has been performed from first principles. Through the use of the supercell method, with quasiharmonic corrections, the vibrational properties of several of these compounds were calculated. Additionally, contributions due to electronic disorder were considered within the one-electron approximation.

In general, there was a good agreement between the calculated and experimental vibrational properties of the structures. Furthermore, it was observed that the phonon DOS of the intermetallics experienced an upward frequency shift,

TABLE VIII. Specific heat of intermetallic compounds in the Mg-Ca-Sn ternary system. From the expression for the Gibbs energy: $G=a+bT+cT\ln(T)+dT^2+eT^3+fT^4+g/T$, the specific heat is given by: $Cp=-c-2dT-6eT^2-12fT^3-2g/T$. Algebraic expression is valid from 298 K up to T_{max}, which corresponds—unless stated otherwise—to the melting temperature.

Compound	c	d $\times 10^{-3}$	e $\times 10^{-6}$	f $\times 10^{-10}$	g $\times 10^{-3}$	T_{max}, K	r^2
fcc Ca	−22.22	−8.62	3.28	−9.03	−2.12	720[a]	0.9999
hcp Mg	−20.35	−10.55	3.45	−9.66	−1.51	933	0.9999
β Sn	−22.85	−8.28	3.40	−14.75	−3.07	505	0.9999
Ca_2Sn	−23.29	−3.14	0.56	−1.11	−1.10	1621	0.9998
Ca_5Sn_3	−23.08	−4.55	1.16	−2.57	−1.17	1510[b]	0.9999
CaSn	−23.08	−4.52	−0.91	−2.01	−1.29	1284	0.9999
$CaSn_3$	−23.08	−6.70	1.24	−5.93	−1.77	903	0.9999
Mg_2Sn	−21.28	−7.16	2.21	−4.99	−1.39	996	0.9998
Mg_2Ca	−21.39	−8.26	2.36	−6.37	−1.49	903	0.9999
MgCaSn	−22.40	−4.74	1.037	−2.30	−1.14	~1500±300[c]	0.9998

[a] This temperature corresponds to the fcc → bcc transition.

[b] This temperature corresponds to the temperature for the peritectic reaction $L+Ca_2Sn \rightarrow Ca_5Sn_3$.

[c] The (metastable) melting temperature for MgCaSn is estimated from the analysis of the Lindemann's constant, f, for the rest of the intermetallic compounds.

relative to the constituent elements due to bond stiffening resulting from the replacement of like with unlike bonds upon compound formation. The results are consistent with the negative entropies of formation obtained for all the intermetallics. Stiffening effects, however, are relatively small, leading to entropies of formation for the compounds which on average were about 10% of the absolute entropies of the constituent elements.

It was also shown that electronic as well as quasiharmonic—i.e., volume expansion—effects contribute with only a fraction of the total free energies, with the former contributions being less significant than the latter. However, the effects of electron disorder on the formation properties increases significantly due to the sharp decrease in the electronic disorder upon compound formation. When studying enthalpy and entropy *differences* between structures, neglecting TEC could have an important effect on the stability of the structures.

The temperature dependence of the formation properties indicates that, except for $CaSn_3$, the compounds become less stable relative to their constituent elements as the temperature increases. The negative change in the quasiharmonic enthalpy and entropy of formation is due to the lower rate of softening of the compounds. It was also observed that the compounds with the more negative enthalpy of formation had in turn more negative entropies of formation. Both quantities are correlated, since they are both indicators of the strengthening of the interatomic bonds upon compound formation.

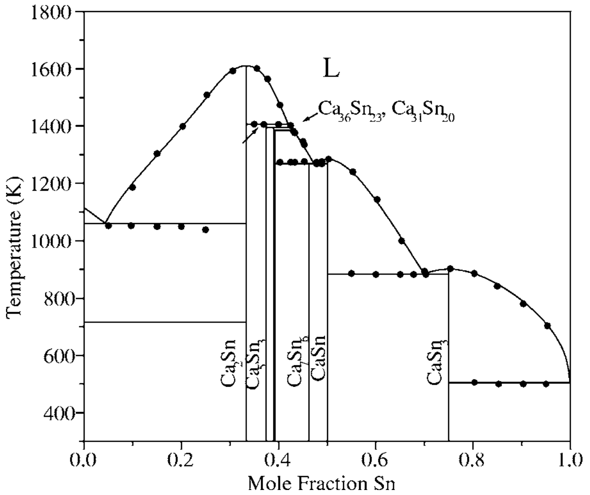

FIG. 8. Calculated (Ref. 14) and experimental (Ref. 12) phase diagram for the Ca-Sn binary system.

ACKNOWLEDGMENTS

The authors would like to thank Alan Luo of General Motors Corporation for the guidance provided to the project. Rainer Schmid-Fetzer is also thanked for the valuable discussions regarding the thermochemistry of the Mg-Ca-Sn system as well as for providing some of the experimental data necessary to validate the present predictions. The authors would like to thank the United States Automotive Materials Partnership (USAMP), consisting of General Motors Corporation, Ford Motor Company, and Daimler-Chrysler Corporation, for their financial support. The authors acknowledge that this research was supported, in whole or in part, by Department of Energy Cooperative Agreement No. DE-FC05-02OR22910. Such support does not constitute an endorsement by the Department of Energy of the views expressed herein. This work is also supported in part by the National Science Foundation (NSF) through Grant No. DMR-0510180. The Materials Simulation Center (MSC) at

Penn State is acknowledged for the computer resources to perform first-principles calculations implemented in VASP, and the LION-XL cluster supported in part by the NSF Grants Nos. (DMR-0205232, DMR-9983532, and DMR-0122638) was also used.

APPENDIX

In order to fully characterize the thermochemical properties of the intermetallic compounds, their Gibbs energies can be reduced through the expression:

$$G = a + bT + cT\ln(T) + dT^2 + eT^3 + fT^4 + g/T, \quad \text{(A1)}$$

from which the following expression for the specific heat is obtained:

$$Cp = -c - 2dT - 6eT^2 - 12fT^3 - 2g/T. \quad \text{(A2)}$$

By knowing the enthalpies of formation, entropies, and specific heats of the structures, their thermochemical properties can be completely be determined. Table VIII shows the coefficients of Eq. (A2) for each of the structures studied in this work. These parameters were simply obtained by fitting the calculated specific heat over the 298-T_{max} range, where the maximum temperature was given by either (metastable) melting points, transition temperatures, or invariant reactions. As can be seen in the table, the correlation is quite reasonable and it can thus be expected that this parametrization can be safely used in the thermodynamic modeling of the compounds in the Mg-Ca-Sn ternary. In fact, recent modeling[14] of the Ca-Sn binary using this precise information has yielded very satisfactory results, as shown in Fig. 8.

---

*Electronic address: raymundo@fastmail.fm

[1] A. L. Bowles, H. Dieringa, C. Blawert, N. Hort, and K. U. Kainer, Mater. Sci. Forum **488-489**, 135 (2005).

[2] G. V. Raynor, *The Physical Metallurgy of Magnesium and Its Alloys*, International Series of Monographs on Metal Physics and Physical Metallurgy (Pergamon Press, New York, 1959), Vol. 5.

[3] A. A. Luo, M. P. Balogh, and B. R. Powell, Metall. Mater. Trans. A **33**, 567 (2002).

[4] K. Ozturk, Y. Zhong, A. A. Luo, and Z.-K. Liu, J. Optim. Theory Appl. **55**, 40 (2003).

[5] Y. Zhong, A. A. Luo, J. O. Sofo, and Z. K. Liu, Mater. Sci. Forum **488-489**, 169 (2005).

[6] N. Saunders and A. P. Miodownik, *CALPHAD (Calculation of Phase Diagrams): A Comprehensive Guide* (Pergamon, New York, 1998).

[7] The CALPHAD method consists of the description of the Gibbs energies of the phases taking part in equilibria in any given system through relatively simple mathematical models.

[8] Y. Zhong, C. Wolverton, Y. A. Chang, and Z.-K. Liu, Acta Mater. **52**, 2739 (2004).

[9] K. Ozturk, Y. Zhong, L. Q. Chen, C. Wolverton, J. O. Sofo, and Z. K. Liu, Metall. Mater. Trans. A **36A**, 5 (2005).

[10] R. Arroyave and Z. K. Liu, CALPHAD: Comput. Coupling Phase Diagrams Thermochem. **30**, 1 (2006).

[11] R. Arroyave, A. van de Walle, and Z. K. Liu, Acta Mater. **54**, 473 (2006).

[12] A. Palenzona, P. Manfrinetti, and M. L. Fornasini, J. Alloys Compd. **312**, 165 (2000).

[13] S. Wei and M. Y. Chou, Phys. Rev. Lett. **69**, 2799 (1992).

[14] M. Ohno, A. Kozlov, R. Arroyave, A. Y. Liu, and Schmid-Fetzer, Acta Mater. **54**, 4939 (2006).

[15] R. Agarwal, J. J. Lee, H. L. Lukas, and F. Sommer, Z. Metallkd. **86**, 103 (1995).

[16] S. Fries and H. L. Lukas, J. Chim. Phys. Phys.-Chim. Biol. **90**, 181 (1993).

[17] M. Ohno, A. Kozlov, R. Arroyave, Z. K. Liu, and R. Schmid-Fetzer (unpublished).

[18] W. Kohn and L. J. Sham, Phys. Rev. **140**, A1133 (1965).

[19] G. Kresse, VASP, Vienna Ab-initio Package Simulation, http://cms.mpi.univie.ac.at/vasp/(2004).

[20] P. E. Blöchl, Phys. Rev. B **50**, 17953 (1994).

[21] G. Kresse and D. Joubert, Phys. Rev. B **59**, 1758 (1999).

[22] J. P. Perdew and A. Zunger, Phys. Rev. B **23**, 5048 (1981).

[23] D. M. Ceperley and B. J. Alder, Phys. Rev. Lett. **45**, 566 (1980).

[24] J. P. Perdew and Y. Wang, Phys. Rev. B **45**, 13244 (1992).

[25] M. Methfessel and A. T. Paxton, Phys. Rev. B **40**, 3616 (1989).

[26] P. E. Blöchl, O. Jepsen, and O. K. Andersen, Phys. Rev. B **49**, 16223 (1994).

[27] A. van de Walle and G. Ceder, Rev. Mod. Phys. **74**, 11 (2002).

[28] A. van de Walle and G. Ceder, J. Phase Equilib. **23**, 348 (2002).

[29] A. van de Walle, M. Asta, and G. Ceder, CALPHAD: Comput. Coupling Phase Diagrams Thermochem. **26**, 539 (2002).

[30] P. H. Dederichs, H. Schober, and D. J. Sellmyer, in *Metals: Phonon States, Electron States and Fermi Surfaces*, edited by K. H. Hellwege and J. L. Olsen (Springer-Verlag, Berlin, 1981), Vol. 13a, Pt. 7 of Landolt-Bornstein, New Series, Group III.

[31] E. F. Skelton, S. T. Lin, and G. M. Rothberg, Acta Crystallogr. **A30**, 39 (1974).

[32] M. Blackman, Acta Crystallogr. **9**, 734 (1956).

[33] V. L. Moruzzi, J. F. Janak, and K. Schwarz, Phys. Rev. B **37**, 790 (1988).

[34] At even higher temperatures, high-order anharmonic effects due to phonon-phonon interactions may become important.

[35] A. A. Quong and A. Y. Liu, Phys. Rev. B **56**, 7767 (1997).

[36] L. A. Grifalco, *Statistical Mechanics of Solids* (Oxford University Press, Oxford, 2000).

[37] T. H. K. Barron, Ann. Phys. (N.Y.) **1**, 77 (1957).

[38] In this work, we have used $\Theta_D(0)$.

[39] M. Asta and V. Ozolins, Phys. Rev. B **64**, 094104 (2001).

[40] Y. Wang, Z.-K. Liu, and L.-Q. Chen, Acta Mater. **52**, 2665 (2004).

[41] C. Kittel, *Introduction to Solid State Physics* (Wiley, New York, 1996).

[42] S. Shang and A. J. Böttger, Acta Mater. **53**, 255 (2005).

[43] J. D. Althoff, P. B. Allen, R. M. Wentzcovitch, and J. A. Moriarty, Phys. Rev. B **48**, 13253 (1993).

[44] R. Ravelo and M. Baskes, Phys. Rev. Lett. **79**, 2482 (1997).

[45] M. J. Winter, WebElements, www.webelements.com(2004).
[46] Q. Chen and B. Sundman, Acta Mater. **49**, 947 (2001).
[47] D. Errandonea, Y. Meng, D. Häusermann, and T. Uchida, J. Phys.: Condens. Matter **15**, 1277 (2003).
[48] J. Ihm and M. L. Cohen, Phys. Rev. B **23**, 1576 (1981).
[49] S. N. Vaidya and G. C. Kennedy, J. Phys. Chem. Solids **31**, 2329 (1970).
[50] R. Schmid-Fetzer, A. Janz, J. Grobner, and M. Ohno, Adv. Eng. Mater. **7**, 1142 (2005).
[51] A. R. Miedema, P. F. de Chatel, and F. R. de Boer, Physica B & C **1000**, 1 (1980).
[52] This approach attempts to estimate the enthalpy of formation of an alloy by considering the charge transfer (negative contribution) and charge density gradients (positive contributions) across the interface between the dissimilar atoms. The numerical estimate of the enthalpies is given by correlations based on the differences in Pauling electronegativity and electron density (Ref. 50).
[53] O. Kubaschewski and H. Villa, Z. Elektrochem. **53**, 32 (1949).
[54] D. J. Min and N. Sao, Metall. Trans. B **19B**, 433 (1988).
[55] X. Q. Chen, W. Wolf, R. Podloucky, and P. Rogl, Intermetallics **12**, 59 (2004).
[56] T. B. Massalski, *Binary Alloys Phase Diagrams*, 2nd edition Vol. 1. (ASM International, 1990).
[57] L. Burakovsky and D. L. Preston, J. Phys. C **65**, 1581 (2004).
[58] J. C. Slater, *Introduction to Chemical Physics* (McGraw-Hill, New York, 1939).
[59] J. S. Dugdale and D. K. C. MacDonald, Phys. Rev. **89**, 832 (1953).
[60] V. Y. Vashchenko and V. N. Zubarev, Fiz. Tverd. Tela (Leningrad) **3**, 886 (1963).
[61] I. Barin, *Thermochemical Data of Pure Substances* (Weinheim, New York, 1995).
[62] At high temperatures, contributions due to thermal defects may also play a role in determining the free energy of a structure. These effects are not considered in this work.
[63] R. Arroyave, M. Ohno, R. Schmid-Fetzer, and Z. K. Liu, in *Magnesium Technology 2006, TMS Fall Meeting*, edited by N. Neelameggham, H. I. Kaplan, and B. R. Powell (TMS, San Antonio, TX, 2006), pp. 429–434.
[64] D. B. Migas, L. Miglio, V. L. Shaposhnikov, and V. E. Borisenko, Phys. Rev. B **67**, 205203(1) (2003).
[65] M. Morishita and K. Koyama, J. Alloys Compd. **398**, 12 (2005).
[66] In Arroyave *et al.* (Ref. 63), the calculated thermodynamic properties of Ca_2Sn and Mg_2Sn from low temperatures until melting were successfully compared with the tabulated thermochemical data (Refs. 61 and 65).
[67] P. Villars, Pauling File, http://crystdb.nims.go.jp/(2004).
[68] A. K. Ganguli, A. M. Guloy, and J. D. Corbett, J. Solid State Chem. **152**, 474 (2000).
[69] A. K. Ganguli, J. D. Corbett, and M. Kockerling, J. Am. Ceram. Soc. **120**, 1223 (1998).
[70] L. Bourdain, thesis, University of Nancy, 1954.
[71] O. Kubaschewski and A. Walter, Z. Elektrochem. **45**, 630 (1939).
[72] O. Kubaschewski and F. Weibke, *Thermochemie der Legierungen* (Springer, Berlin, 1943).
[73] P. Beardmore, B. W. Howlett, B. D. Lichter, and M. B. Bever, Trans. AIME **236**, 102 (1966).
[74] A. Borsese, B. G., R. Ferro, and Capelli, Z. Metallkd. **66**, 226 (1975).
[75] R. C. King and O. J. Kleppa, Acta Mater. **12**, 87 (1964).
[76] G. J. Gartner, thesis, Iowa State University, 1965.
[77] J. E. Davison and J. F. Smith, Trans. Metall. Soc. AIME **242**, 2045 (1968).
[78] C. J. Buchenauer and M. Cardona, Phys. Rev. B **3**, 2504 (1971).
[79] B. G. Childs, Rev. Mod. Phys. **25**, 665 (1953).